J Solid State Electrochem (2010) 14:1351–1358
DOI 10.1007/s10008-009-0958-3

ORIGINAL PAPER

Nanostructured nickel (II) phthalocyanine—MWCNTs as viable nanocomposite platform for electrocatalytic detection of asulam pesticide at neutral pH conditions

Msimelelo P. Siswana · Kenneth Ikechukwu Ozoemena · Daniela A. Geraldo · Tebello Nyokong

Received: 8 April 2009 / Revised: 22 July 2009 / Accepted: 10 October 2009 / Published online: 6 November 2009

Abstract This work reports for the first time that nanostructured nickel (II) phthalocyanine/multiwalled carbon nanotubes composite supported on a basal plane pyrolytic electrode (NiPcNP/MWCNT-BPPGE) could potentially serve as a viable platform for the sensitive electrocatalytic detection of asulam pesticide at phosphate-buffered solution (pH 7.0 conditions). Comparative electron transfer dynamics, using ferrocyanide/ferricyanide as outer sphere redox probe, were examined and interpreted using the Davies–Compton theoretical framework dealing with voltammetry at spatially heterogeneous electrodes. The NiPcNP/MWCNT-BPPGE exhibits fast electron transport and excellent electrocatalytic behavior toward asulam, with an onset potential of about 150 mV lower than observed for the electrode without MWCNTs or bare BPPGE. Also, NiPcNP/MWCNT-BPPGE displayed good analytical performance for asulam, with a detection limit of 0.285 μM, a linear concentration range of 91–412 μM, and a sensitivity of 44.6 μA mM^{-1}.

Keywords Asulam · Nickel phthalocyanine · Cyclic voltammetry · X-ray photoelectron spectroscopy · Nanoparticles · Carbon nanotubes

M. P. Siswana · D. A. Geraldo · T. Nyokong
Department of Chemistry, Rhodes University, Grahamstown 6140, South Africa

K. I. Ozoemena (✉)
Materials Science and Manufacturing, Council for Scientific and Industrial Research (CSIR), Pretoria 0001, South Africa
e-mail: kozoemena@csir.co.za

Introduction

The use of nanosized materials as catalysts has found widespread application in many areas of chemistry. In electrochemistry, these materials have also been used as electrode modifiers. Nanoparticle-modified electrodes can display unique advantages over macroelectrodes when used for electroanalysis. These include high-effective surface area, improved mass transport, catalysis, and control over local environment [1].

Carbon nanotubes have had a profound impact on diverse areas of scientific and technological research, including in electrochemistry. Their unique electrical properties, high-chemical stability, and high-surface to volume ratio have been the subject of many investigations [2–4]. Functionalization of carbon nanotubes with various kinds of materials is gaining more attention as the different properties of the attached functionalities are required for specific applications [5–7].

The work described in this paper is part of our program in the search for novel electrocatalytic platforms based on metallophthalocyanines (MPcs) integrated with carbon nanotubes (CNTs) for the purpose of electrochemical detection of herbicides that are potentially toxic. When compared to other transition MPcs (notably FePc and CoPc complexes), NiPc derivatives are the least investigated as electrocatalysts for analytes such as the herbicide, asulam [8, 9]. This is because, while the central metals of the CoPc and FePc complexes exhibit excellent redox-activity, the central metal of NiPc is inherently redox-inactive (redox-silent) during electrocatalytic studies. In this work, we probe for the first time, the electrocatalytic activity of NiPc nanoparticles integrated with multiwalled carbon nanotubes (MWCNTs) for the detection of asulam. Our choice for the

nanoparticles of NiPc for this study is motivated by the envisaged enhanced electrocatalytic properties for high-surface area metallophthalocyanine nanoparticle species as well as the novelty of nanostructured NiPc for asulam detection. We are not aware of any report on the synthesis of NiPc nanoparticles (NiPcNP) or its use as an electrocatalyst for the detection of any herbicide. Asulam is a carbamate pesticide which is most often used as a postemergence herbicide for controlling deciduous and perennial grasses. It exhibits a high mobility by virtue of the high-water solubility of its sodium salt and is therefore a potential pollutant [10].

Experimental

Materials, reagents, and nonelectrochemical instrumentation

Asulam and MWCNTs were obtained from Sigma. Dimethyl sulphoxide, potassium ferricyanide, and potassium ferrocyanide were obtained from SAARCHEM (Midrand, South Africa). The basal plane pyrolytic graphite (BPPG) from which the basal plane pyrolytic graphite electrode (BPPGE) was constructed in-house was obtained from Le Carbone (Sussex, UK). The Norton Caborundum Paper (p1200 c) used to clean the electrode was purchased from Saint Gobain Abrasives (Saint-Gobain Abrasives (pty) Ltd., Isando, South Africa). Ultra pure water of resistivity 18.2 MΩ cm was obtained from Milli-Q Water Systems (Millipore Corp., Bedford, MA, USA) and was used throughout for the preparation of solutions. All other reagents such as dipotassium hydrogen orthophosphate, potassium dihydrogen orthophosphate, phosphoric acid, and sodium hydroxide were of analytical grade and were used as received without further purification. Phosphate buffer solutions (PBS) were prepared with appropriate amounts of K_2HPO_4 and KH_2PO_4 and the pH adjusted with 0.1 M H_3PO_4 or NaOH. The nickel phthalocyanine was synthesized and characterized according to established procedures [11]. X-ray photoelectron spectra (XPS) were recorded with a Physical Electronics model 5400 spectrometer system equipped with an Mg/Al dual source and a small area analyzer with PSD detector. An achromatic Mg K X-ray (1,253.6 eV) source was operated at 300 W. Indium oxide was used as the substrate.

Electrochemical methods

All electrochemical experiments were performed with an Autolab Potentiostat PGSTAT 30 (Eco Chemie, Utrecht, The Netherlands) driven by a General Purpose Electrochemical Systems data processing software (GPES, software version 4.9). Electrochemical impedance spectroscopy (EIS) measurements were performed between 1.0 Hz and 10 kHz using a 10 mV rms sinusoidal modulation in a solution of 1 mM $K_4Fe(CN)_6/K_3Fe(CN)_6$ (1:1) mixture in 0.1 M PBS (pH 7.0) and at the $E_{1/2}$ of the $[Fe(CN)_6]^{3-/4-}$ (0.2 V vs Ag|AgCl wire). The frequency response analyzer software allowed the fitting of the raw EIS data to equivalent circuit models using a *complex nonlinear least squares* routine, with *Krammers–Kronig rule check*. A conventional three-electrode system was used. The basal plane pyrolytic graphite electrode disk (d=5 mm in Teflon) used as working electrode was fabricated in-house by the Rhodes University Chemistry Machinery Workshop. Electrical contact with the disk was obtained via an inserted copper wire held in place with conducting silver varnish L 100 (Kemo® Electronic, Germany). The working electrode was an unmodified BPPGE or BPPGE modified with (a) MWCNTs (MWCNT-BPPGE), (b) NiPcNP (NiPcNP-BPPGE), and (c) the physically mixed MWCNT/NiPcNP nanocomposite (MWCNT/NiPcNP-BPPGE). The normal Ag|AgCl (3 M KCl) electrode was used as reference electrode and a platinum wire as counter electrode. A Wissenschaftlick–Technische Werkstätten pH 330/set 1 (Germany) pH meter was used for pH measurements.

Synthesis of NiPc nanoparticles

The nanoparticles were synthesized as described previously for nanoCoPc [12] with a slight modification. Briefly, 0.15 g NiPc was dissolved in 5 ml of 98% concentrated sulfuric acid. The solution was then added drop-by-drop into a vigorously stirred 300 ml aqueous solution containing 0.45 g hexadecyltrimethyl ammonium-chloride (CTACl; $C_{16}H_{33}N(CH_3)_3Cl$). The resulting solution was centrifugally separated. The obtained sedimentation was washed repeatedly to neutral with water. It was then dried in air to obtain the nanoNiPc powder.

Purification of multiwalled carbon nanotubes

The MWCNTs were purified as described previously [13]. Briefly, 1 g of MWCNTs was added to 140 ml of 2.6 M HNO_3, and the mixture was refluxed for 45 h. The carbon nanotube sediment was separated from solution and washed with distilled water. It was then sonicated in a 3:1 mixture of H_2SO_4 and HNO_3 for 24 h. The sediment was thereafter washed with distilled water, stirred for 30 min in a 4:1 H_2SO_4/H_2O_2 mixture at 70 °C, and washed with distilled water. The purified MWCNT paste was then air-dried for 48 h.

Attachment of NiPcNP to carbon nanotubes

The NiPc nanoparticles were physically attached to the MWCNTs by mixing 1 mg of MWCNTs with 5 mg of

NiPcNP in 10 ml of water, then stirring for 2 h, forming a NiPcNP/MWCNT nanocomposite [14]. The NiPcNP/MWCNT nanocomposite was separated from solution by filtration and air-dried for 48 h to form a powder.

Electrode pretreatment and modification

A BPPGE was prepared for use or for further modification by renewing the electrode surface with cellotape [15]. This procedure involves polishing an old BPPGE surface on carborundum paper, pressing cellotape on the cleaned BPPGE surface, and then removing the tape, along with several layers of graphite. Before use, the electrode was rinsed in acetone to remove any adhesive. To prepare modified electrodes, MWCNTs or NiPcNP/MWCNT nanocomposite were attached to the BPPGE surface by gently rubbing the electrode on a high-quality filter paper containing either of these materials [16]. Experiments were also conducted where NiPcNP was adsorbed on the electrode in the absence of MWCNT (represented as NiPcNP-BPPGE). To prepare these electrodes, NiPcNPs were attached to the BPPGE surface in the manner discussed above [16], except that the filter paper contained NiPcNPs instead of the other materials.

Results and discussion

Characterization

Figure 1 shows comparative X-ray photoelectron spectra of the NiPcNP/MWCNTs and MWCNTs. In the photoelectron spectrum of the MWCNTs the C 1s peak is located at 284.4 eV, attributed to the C–C bonds of the MWCNTs.

The other dominant peak is the O 1s peak at 532.3 eV, which is due to the O–H bond within the carboxyl group of the acidified MWCNTs. The small peak at 533 eV is an O

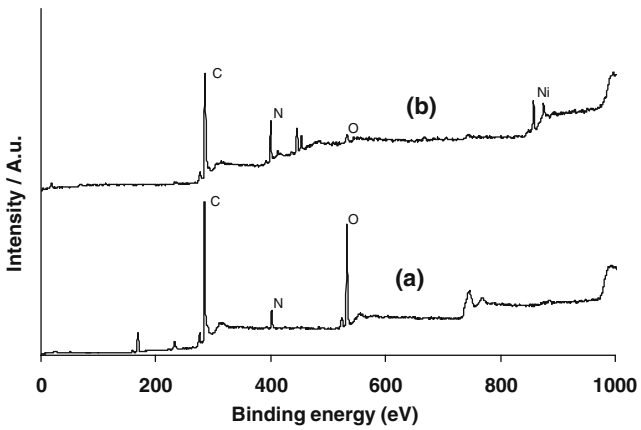

Fig. 1 X-ray photoelectron spectra of MWCNTs (*a*) and NiPcNP/MWCNTs (*b*)

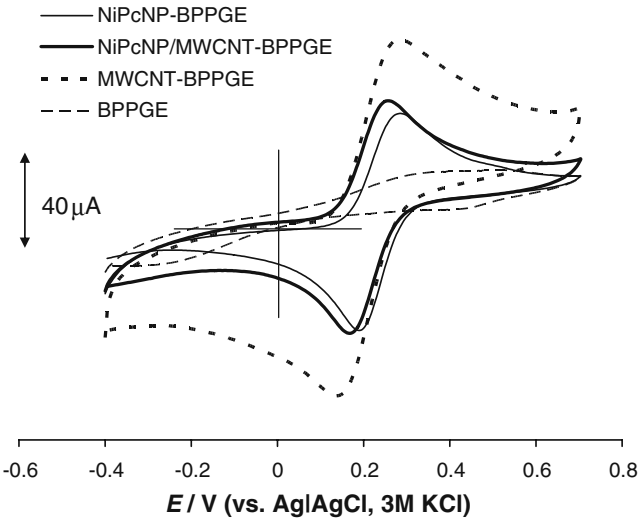

Fig. 2 Comparative cyclic voltammetric evolutions of different electrodes recorded in 10^{-3} M $[Fe(CN)_6]^{4-}/[Fe(CN)_6]^{3-}$ with 0.1 M PBS (pH 7.0) as the supporting electrolyte. Scan rate=50 mV s^{-1}

1s peak attributed to the C=O bond of the carboxyl group of MWCNT. The small N 1s peak at about 400 eV (for MWCNT) may be due to nitrogen located either within the phthalocyanine complex from which most of the MWCNTs are reported to be synthesized [17] or in the traces of nitric acid remaining within the MWCNTs after the purification process. The XPS spectrum of NiPcNP/MWCNTs shows a C 1s peak at 285.05 eV. This peak is due to the C–C bonds of the MWCNTs and the NiPcNPs. An N 1s peak due to the C–N bonds of the NiPcNPs also appears at 399.7 eV. The double peak appearing at ~445 eV is due to the indium oxide substrate (as has been reported before [18, 19]) on which the NiPcNP/MWCNTs powder is placed for analyses purposes. This peak is not clear in the MWCNT spectrum due to the different nature of the samples. This means that the powder forms either islands or a very thin layer on the surface, thus exposing the indium oxide surface to analysis as well [18]. The small O 1s peak at 532 eV is probably due to the oxygen in the indium oxide substrate [19]. The Ni $2p_{3/2}$ peak appears at 857.5 eV, and the Ni $2p_{½}$ peak appears at 874.5 eV.

Comparative electron transfer kinetics

Figure 2 shows the cyclic voltammograms for the bare BPPGE, MWCNT-BPPGE, NiPcNP/MWCNT-BPPGE, and NiPcNP-BPPGE recorded in phosphate buffer solution (pH 7.0) containing 1 mM $[Fe(CN_6)]^{3-}/[Fe(CN_6)]^{4-}$ redox probe. The bare BPPGE did not show any significant response.

As expected for the high-surface area MWCNTs, the cyclic voltammogram of the MWCNT-BPPGE is characterized by huge capacitive (background) current compared to those based on the NiPcNP. The potential peak-to-peak

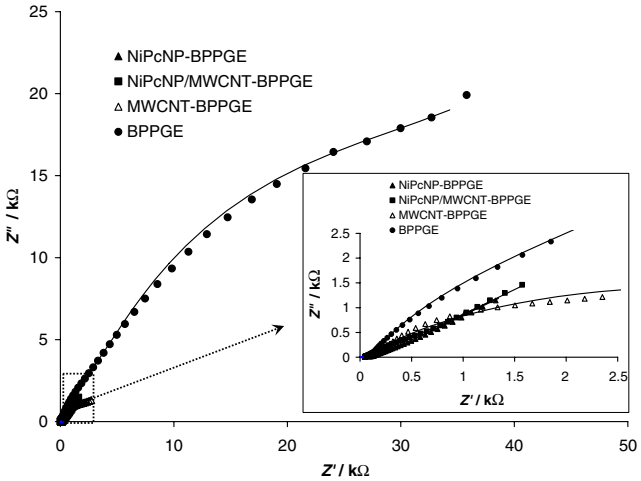

Fig. 3 Comparative Nyquist plots of the different electrodes recorded in 0.1 M PBS (pH 7.0) containing 10^{-3}M $[Fe(CN)_6]^{4-}/[Fe(CN)_6]^{3-}$ at a fixed potential of 0.2 V (vs Ag|AgCl wire). The *symbols* represent the experimental data, while *solid lines* are fitted curves using equivalent circuits shown in Fig. 4

separation (ΔE_p) decreases as MWCNT-BPPGE (166 mV) > NiPcNP-BPPGE (107 mV) ≈ NiPcNP/MWCNT-BPPGE (103 mV), suggesting that the two NiPcNP based electrodes facilitate electron transfer kinetics of the redox probe in solution than the MWCNT-BPPGE or BPPGE. The ratio of the cathodic faradaic current/background current increases as MWCNT-BPPGE (~1.6) < NiPcNP/MWCNT-BPPGE (~1.8) < NiPcNP-BPPGE (~3.0), which essentially corroborates the ΔE_p data. Note that the background or capacitive current was measured at the –0.2 V. The ratio of the anodic faradaic current/background current for the MWCNT-BPPGE (~6.5) was essentially the same (~6.6) as estimated for the two NiPcNP-based electrodes.

Davies and Compton [20] elegantly developed theoretical framework for dealing with voltammetry at spatially heterogeneous electrodes or diffusion at microelectrode arrays. From this particular work [20] and related works from the same group [21, 22], the voltammogram of the MWCNT-BPPGE may be assigned to the type 4 behavior (i.e., planar/linear diffusion, wherein the diffusion layer thickness, δ, is much larger than the insulating layer leading to a complete or heavily overlapping of the adjacent diffusion layers and a linear concentration profile). The CVs of the two NiPcNP-based electrodes (NiPcNP/MWCNT-BPPGE and NiPcNP-BPPGE) are typical behavior of nonlinear diffusion process where the individual diffusion layers do not overlap (type 2 behavior) or weakly overlap (type 3 behavior). If we consider the cathodic faradaic current/background current ratios, NiPcNP-BPPGE that exhibits the highest ratio will be assigned to type 2 while NiPcNP/MWCNT is due to type 3 [20, 21]. The apparent increase in current at the MWCNT-BPPGE is somewhat surprising, but the answer may be found in the recent work of Compton and coworkers [23], where the authors showed that the cyclic voltammetry recorded at CNT-based electrodes involves semi-infinite linear diffusion and thin layer diffusion processes, the latter process arising from the oxidation of trapped electrolytes within the CNT porous layers.

Since electrochemical impedance spectroscopy provides a more detailed description of an electrochemical system than cyclic voltammetry does [24, 25]. EIS was further used to follow the electron transfer kinetics occurring at these electrodes. The EIS measurements were performed at the formal potential ($E_{1/2}$≈210 mV) of the $[Fe(CN)_6]^{4-}/[Fe(CN)_6]^{3-}$ as recorded in the CVs (Fig. 2). Figure 3 shows examples of the Nyquist plots obtained for the electrodes in the $[Fe(CN)_6]^{4-}/[Fe(CN)_6]^{3-}$ solution.

An essential aspect of EIS is the ability to fit the spectral data with some theoretical electrical equivalent circuit models. As seen in Fig. 4 (data summarized in Table 1), the electrodes were satisfactorily fitted with the proposed equivalent circuits judged by the relative percent errors and visual inspection of the fitted lines as well as the pseudo-χ^2 ($\leq 10^{-4}$) from the Kramer–Kronig test. The bare BPPGE was fitted with the modified Randles equivalent circuit incorporating one Voigt circuit (Fig. 4 a); the NiPcNP-BPPGE and NiPcNP-MWCNT-BPPGE were both fitted with equivalent circuits shown in Fig. 4 b, while the MWCNT-BPPGE was fitted with equivalent circuit shown

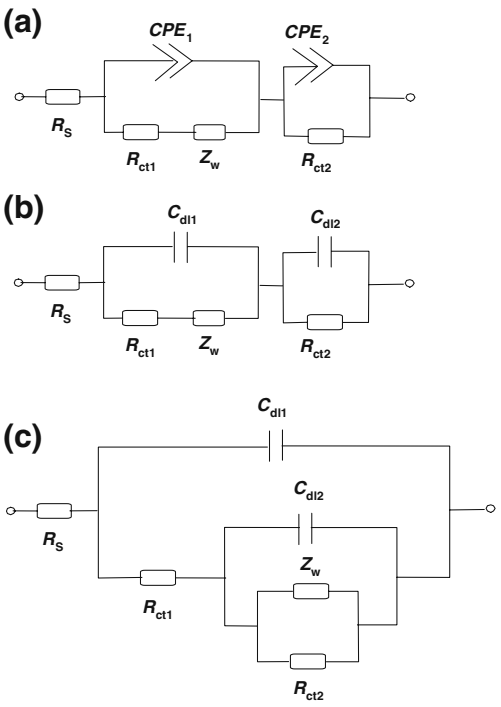

Fig. 4 Equivalent circuits used to fit the EIS data of Fig. 3. Circuit was used for the bare BPPGE (*a*), was used for the two NiPcNP-based electrodes (*b*), and was used for the MWCNT-BPPGE (*c*)

Table 1 Impedance data for the electrodes recorded in $[Fe(CN)_6]^{4-}/[Fe(CN)_6]^{3-}$ at 0.2 V (vs Ag|AgCl wire)

EIS parameters	Electrode			
	BPPGE	NiPcNP-BPPGE	MWCNT-BPPGE	NiPcNP-MWCNT-BPPGE
R_s/Ω	94.2 (1.76)	74.1 (2.54)	77.9 (6.71)	44.9 (0.63)
$CPE_1/\mu F$	14.5 (5.91)			
n_1	0.75 (6.26)			
$CPE_2/\mu F$	9.95 (6.72)			
n_2	0.79 (5.89)			
$R_{ct1}/k\Omega$	38.4 (14.79)	0.038 (4.31)	0.057 (8.78)	0.0095 (4.52)
$Z_w/\mu\Omega$	79.5 (14.27)	751 (1.06)	254 (4.76)	624 (0.35)
$R_{ct2}/k\Omega$	2.39 (36.16)	0.045 (8.17)	6.51 (11.66)	0.089 (3.20)
$C_{dl1}/\mu F$		0.84 (10.76)	0.85 (22.79)	2.57 (5.86)
$C_{dl2}/\mu F$		113.3 (11.45)	20.11 (9.6)	502 (2.96)

Value in parenthesis is the percent fitting errors used in the equivalent circuits in Fig. 4

in Fig. 4 c. The fitting parameters involve the electrolyte resistance (R_s), electron-transfer resistance (R_{ct}), constant phase element (CPE) due to the inherent roughness of the electrode, double-layer capacitance (C_{dl}) associated with the electrode surface, and Warburg-type impedance (Z_w) which is associated with the diffusion of the ions of the redox probe.

Within the limits of errors, the effective charge transport resistance (i.e., summation of the charge-transfer resistances in series connection, R_{ct1} and R_{ct2}) of each of the electrode approximately follows as: bare BPPGE (~41 kΩ) > MWCNT-BPPGE (~7 kΩ) > NiPcNP-MWCNT-BPPGE (~0.1 kΩ) ≈ NiPcNP-BPPGE (~0.1 kΩ). The key observation here is that the electron-transfer processes at the NiPcNP-based electrodes are much faster than seen at the bare BPPGE or the MWCNT-BPPGE, excellently corroborating the results from the CV experiments discussed above. This observation is also in good agreement with a recent study on SWCNT and CoPcNP [26].

The enhanced electron transport exhibited by the two NiPcNP-based electrodes may be related to any or all of the three following processes. First, it is well documented that redox-inactive and noncatalytic materials, for example, bulk gold, become catalytic when converted to their nanostructures. Thus, it may be true that upon nanostructuring, the redox-silent and noncatalytic central Ni of the NiPc become redox-active and catalytic. Second, the protection of the NiPcNP with positively charged CTACl plays a role in the electron transportation by its electrostatic interaction with the negatively charged $[Fe(CN)_6]^{4-}/[Fe(CN)_6]^{3-}$. Note that our acid-functionalized MWCNTs are negatively charged, hence, poor activity of the MWCNT-BPPGE due to some repulsive interaction with the redox probe. Third, the MWCNT/NiPcNP enhanced electron transport in a synergistic fashion, MWCNTs acting as electron conducting nanowires, while the NiPcNP acting as the electrocatalyst. Although there is no significant difference in the electron transfer behavior of the NiPcNP and MWCNT/NiPcNP, the catalytic activity of the latter is best observed in the electrocatalytic detection of asulam (discussed later).

The impedance of the CPE (Z_{CPE}) is defined as in Eq. 1:

$$Z_{CPE} = [Q(j\omega)^n]^{-1} \quad (1)$$

where Q is the frequency-independent constant relating to the interface, $j=\sqrt{-1}$, ω is the radial frequency, the exponent n arises from the slope of log Z vs log f (and has values $-1 \leq n \leq 1$). If $n=0$, the CPE behaves as a pure resistor; $n=1$, CPE behaves as a pure capacitor; $n=-1$, CPE behaves as an inductor; while $n=0.5$ corresponds to Warburg impedance (Z_w). From Table 1, the two n values recorded for the BPPGE fall between 0.75 and 0.79, meaning, pseudocapacitive behavior. From the Bode plots (Fig. 5), the slopes of the log Z vs log f plot at the midfrequency region are less than the ideal –1.0 for pure capacitive behavior, which is indicative of pseudocapacitive behavior. Also, from the other Bode plot (i.e., –phase angle (ϕ) vs log f), the phase angles are less than the 90° expected of an ideal capacitive behavior, confirming the pseudocapacitive behavior.

It should be stresssed here that every attempt to replace the C_{dl} with a CPE in the modeling circuit led to huge errors. This does not mean that the C_{dl} is a pure double-layer capcitance. According to Orazem and Tribollet [27], frequency dispersion leading to CPE behavior occurs via two processes; distribution of time constants along either the area of the electrode surface (involving a two-dimensional (2-D) aspect of the electrode) or along the axis normal to the electrode surface (involving a three-dimensional surface). Importantly, a 2-D distribution presents itself as an ideal RC behavior. Thus, we may conclude here that the observed impedimetric behavior of the modified electrodes most likely involves time constant distributions occuring along the area of the electrode as well as along the axis normal to the electrode. The data from the Bode plots further confirms the absence of ideal capacitive behavior.

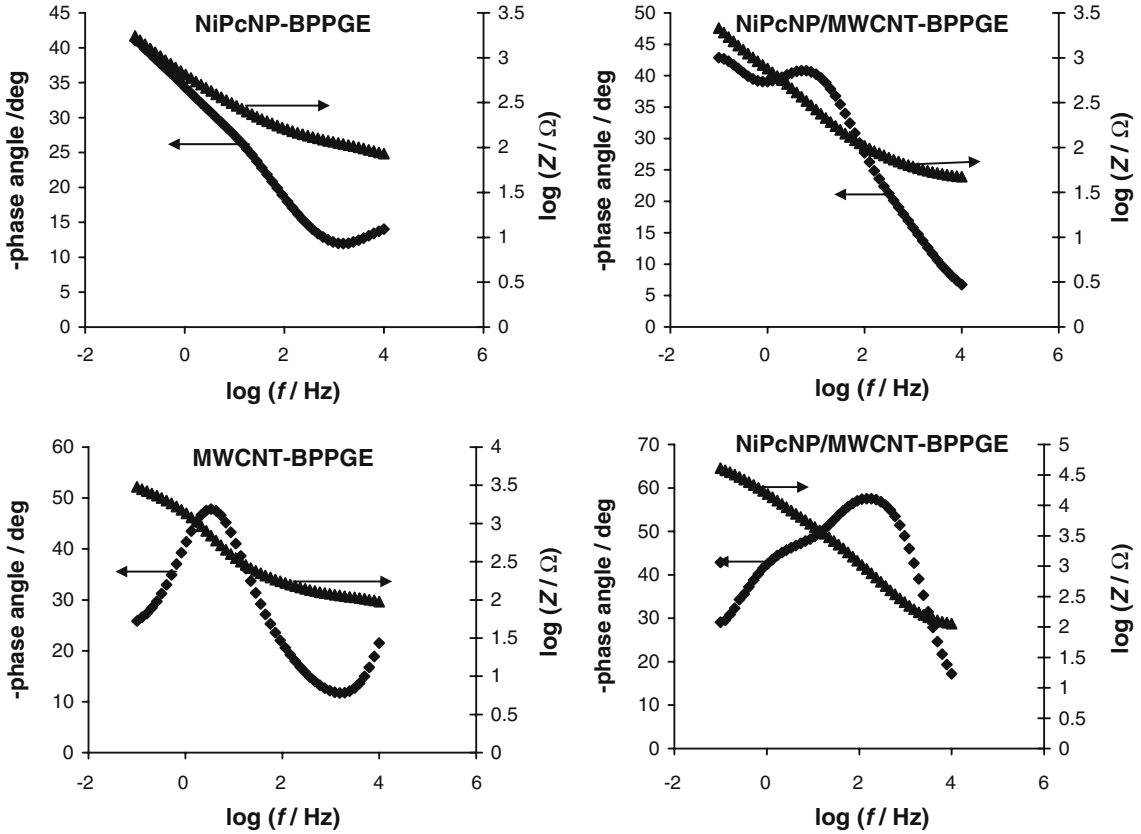

Fig. 5 Comparative Bode plots of the different electrodes recorded in 0.1 M PBS (pH 7.0) containing 10^{-3} M $[Fe(CN)_6]^{4-}/[Fe(CN)_6]^{3-}$ at a fixed potential of 0.2 V (vs Ag|AgCl wire). The *symbols* represent the experimental data, while *solid lines* are fitted curves using equivalent circuits shown in Fig. 4

Comparative electrocatalysis of asulam

Figure 6 shows the comparative background-corrected current cyclic voltammograms of the BPPGE, NiPcNP-BPPGE, and NiPcNP/MWCNT-BPPGE recorded in 0.1 M PBS (pH 7.0) containing 1×10^{-3}M asulam. Electrocatalysis is defined as the reduction in energy (potential).

It is clearly seen that NiPcNP/MWCNT-BPPGE gave the best electrocatalytic behavior as its onset potential (~0.65 V) is about 150 mV lower than the other electrodes that occurred at approximately 0.8 V. MWCNT-BPPGE is known to show poor activity toward asulam [9]. In this potential region, it is expected that ring oxidation of the NiPc will occur [28, 29]. The ring oxidation process may assist electron transfer between asulam and the NiPcNP-MWCNT-BPPG electrode surface as proposed in the following mechanism:

$$NiPc^{2-} \rightarrow \left[NiPc^{-1}\right]^{+} + e^{-} \quad (2)$$

$$\left[NiPc^{-1}\right]^{+} + \text{asulam} \rightarrow NiPc^{2-} + \text{asulam oxidation product} \quad (3)$$

The enhanced catalysis observed at the NiPcNP/MWCNT-BPPGE is attributed to the nanocomposite nature of the NiPc/MWCNTs as already explained in the discussion on electron transport. Thus, all further investigations were performed with NiPcNP/MWCNT-BPPGE. A plot of I_{pa} against $\nu^{1/2}$ (not shown) resulted in a straight

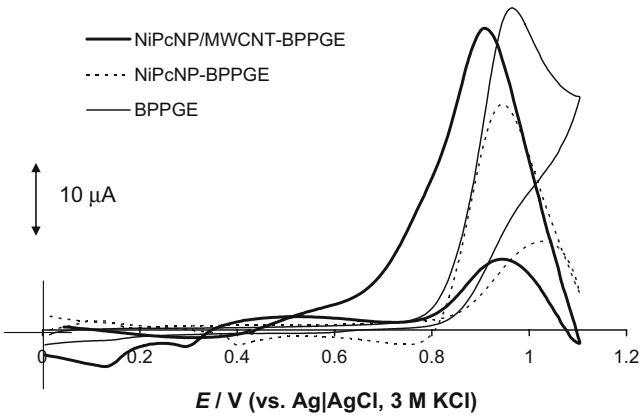

Fig. 6 Background-corrected cyclic voltammograms for BPPGE, NiPcNP-BPPGE, and NiPcNP/MWCNT-BPPGE in 1×10^{-3}M asulam. MWCNT-BPPGE is removed for clarity. Supporting electrolyte is 0.1 M phosphate buffer at pH 7.0

line, showing that for this electrode, asulam oxidation is diffusion-controlled. A plot of $I_{pa}/\nu^{1/2}$ against ν (Fig. 7) resulted in the characteristic shape that is typical of a catalytic process [30].

Chronoamperometric detection of asulam

Given the best performance exhibited by the NiPcNP/MWCNT-BPPGE, the electrode was employed to test for chronoamperometric detection of asulam in pH 7.0 conditions (exemplified in Fig. 8) at a fixed potential of 0.92 V (vs Ag|AgCl, 3 M KCl).

The plot was linear over the concentration range of 91–412 μM with a sensitivity of 44.6 μA mM^{-1} and a detection limit of 0.285 μM (using the $Y_B+3\sigma$ criterion). It is noteworthy that NiPcNP/MWCNT-BPPGE displayed a comparable or even better analytical data to reported works such as for *poly*-cobalt tetra-aminophthalocyanine-modified MWCNT-BPPGE [9] that gave a detection limit of 1.15 μM, or the detection limits of 7 and 1.7 μM recorded for asulam at a glassy carbon electrode [31] and a glassy carbon electrode coupled to a capillary electrophoresis instrument [32], respectively.

We examined the stability of this electrode by studying the impact of scan number on the current response (exemplified in Fig. 9). The plot shows that the current response decreases to 42% of its initial value after about the fourth scan and then stabilizes. Also, 86% of the initial current response is recovered upon rinsing of the electrode in phosphate buffer at pH 7. Furthermore, if the electrode is rinsed and then left in the refrigerator for 2 weeks, 91% of the initial current response is displayed.

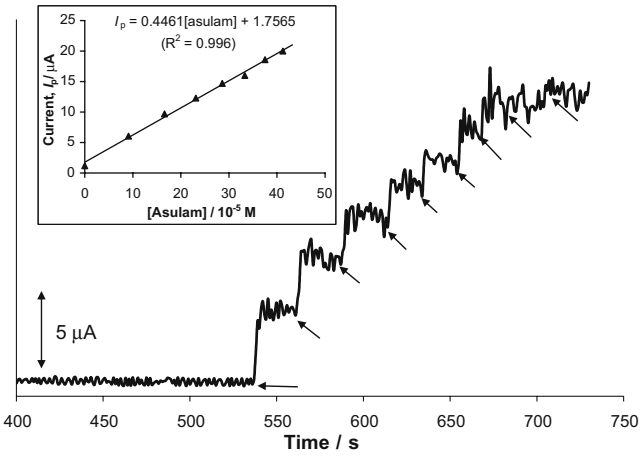

Fig. 8 Chronoamperograms recorded on sequential injection of aliquots of asulam (1 ml of 1×10^{-3}M) to pH 7 buffer using NiPcNP/MWCNT-BPPGE. The *arrows* in the chronoaperograms indicate points of injection. *Inset* is plot of I_P vs *[Asulam]*

Conclusion

For the first time, the electrochemical activity of nanocomposite mixture of NiPc and MWCNTs has been described. The nanocomposite improves the electrochemical response of the ferri/ferrocyanide redox probe and greatly enhanced the electrocatalytic response of asulam at neutral pH conditions. The ease of fabrication of the NiPcNP/MWCNT-BPPGE combined with its high sensitivity and low-detection limit in the presence of asulam makes it a very attractive and viable nanocomposite platform for electrochemical detection of this herbicide.

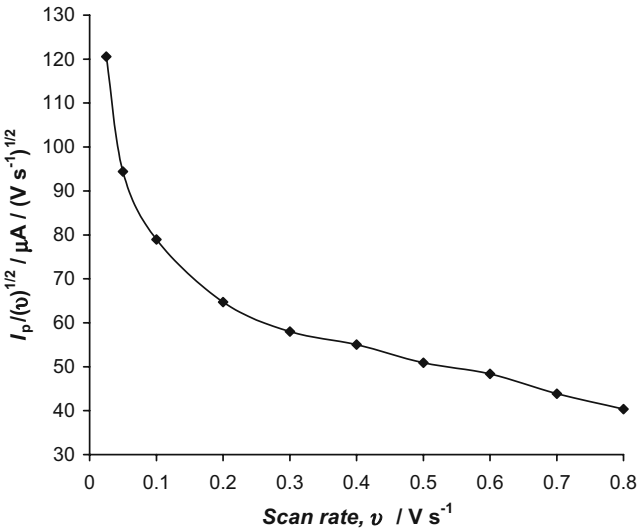

Fig. 7 Plot of $I_P/\nu^{1/2}$ vs ν for the catalytic oxidation of asulam on NiPcNP/MWCNT-BPPGE

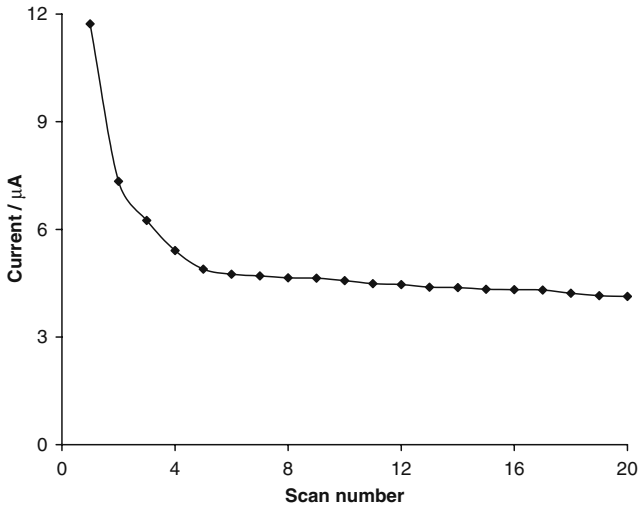

Fig. 9 Impact of scan number on the catalytic current response of a 1-mM asulam at the NiPcNP/MWCNT-BPPGE

Acknowledgments We thank Rhodes University, the Department of Science and Technology (DST) and National Research Foundation (NRF) through the DST/NRF Research chair initiatives for funding. MS thanks Walter Sisulu University for a graduate scholarship. KIO thanks CSIR and NRF for their support.

References

1. Welch CM, Compton RG (2006) Anal Bioanal Chem 384:601
2. Dieckmann GR, Dalton AB, Johnson PA, Razal J, Chen J, Giondano J (2003) J Am Chem Soc 125:1770
3. Hrapovic S, Líu KB, Luong JHT (2004) Anal Chem 76:1083
4. Luo H, Shi Z, Li N, Gu Z, Zhuang Q (2001) Anal Chem 73:915
5. de la Torre G, Blau W, Torres T (2003) Nanotechnology 14:765
6. Rubiens MD, Rivas GA (2003) Electrochem Commun 5:689
7. Wang J, Musameh M (2003) Anal Lett 36:2041
8. Siswana MP, Ozoemena KI, Nyokong T (2006) Talanta 69:1136
9. Siswana MP, Ozoemena KI, Nyokong T (2006) Electrochim Acta 52:114
10. Chivulescu A, Catalá-Icardo M, García Mateo JV, Martínez Calatavud J (2004) Anal Chim Acta 519:113
11. Metz J, Schneider O, Hnack M (1984) Inorg Chem 23:1064
12. Yang G-J, Wang K, Xu J-J, Chen H-Y (2004) Anal Lett 37:629
13. Liu J, Rinzler AG, Dai H, Hafner JH, Kelley Bradley R, Boul PJ, Lu A, Smalley RE (1998) Science 280:1253
14. Yang M, Yang Y, Qu F, Lu Y, Shen G, Yu R (2006) Anal Chim Acta 571:211
15. Salimi A, Compton RG, Hallaj R (2005) Anal Biochem 333:49
16. Moore RR, Banks CE, Compton RG (2004) Anal Chem 76:2677
17. Yudasaka M, Kikuchi R, Ohki Y, Yomishura S (1997) Carbon 35:195
18. Ureta-Zañartu MS, Berrios C, Pavez J, Zagal J, Gutiérrez C, Marco JF (2003) J Electroanal Chem 553:147
19. Brumbach M, Veneman PA, Marrikar FS, Schulmeyer T, Simmonds A, Xia W, Lee P, Armstrong NR (2007) Langmuir 23:11089
20. Davies TJ, Compton RG (2005) J Electroanal Chem 585:63
21. Davies TJ, Banks CE, Compton RG (2005) J Solid State Electrochem 9:797
22. Dai X, Wildgoose GG, Salter C, Crossley A, Compton RG (2006) Anal Chem 78:6102
23. Streeter I, Wildgoose GG, Shao L, Compton RG (2008) Sens Actuator B 133:462
24. Mamuru SA, Ozoemena KI (2009) Mater Chem Phys 114:113
25. Pillay J, Ozoemena KI (2009) Electrochim Acta 54:5053
26. Agboola BO, Mocheko A, Pillay J, Ozoemena KI (2008) J Porphyrins Phthalocyanines 12:1289
27. Orazem ME, Tribollet B (2008) Electrochemical impedance spectroscopy, chapter 13. Wiley, Hoboken
28. Li H, Guarr TH (1989) J Chem Soc Chem Commun 832
29. Li H, Guarr TH (1991) J Electroanal Chem 317:189
30. Golabi SM, Zare HR (1999) J Electroanal Chem 465:168
31. Nouws HPA, Delerue-Matos C, Lima JLFC, Garrido EM, Vincke P, Maes NA (2002) Int J Environ Anal Chem 82:69
32. Chicharro M, Zapardiel A, Bermejo E, Sanchez A (2002) Anal Chim Acta 469:243